



Adam B Sokol<sup>1</sup>, Casey J Wall<sup>2</sup>, and Dennis L Hartmann<sup>1</sup>

<sup>1</sup>Department of Atmospheric Sciences, University of Washington

<sup>2</sup>Department of Geosciences, University of Oslo

February 16, 2024

## Abstract

High clouds produced by tropical convection are expected to shrink in area as climate warms, and the radiative feedback associated with this change has long been the subject of controversy. In a recent assessment of climate sensitivity, the World Climate Research Programme (WCRP) estimated that the feedback is significantly negative, albeit with substantial uncertainty. Here we show that such a negative feedback is not supported by an ensemble of high-resolution atmospheric models. Rather, the models suggest that changes in cloud area and opacity act as a modest positive feedback. The positive opacity component arises from the disproportionate reduction in the area of thick, climate-cooling clouds relative to thin, climate-warming clouds. This suggests that thick cloud area is tightly coupled to the rate of convective overturning—which is expected to slow with warming—whereas thin cloud area is influenced by other, less-certain processes. The cloud response is examined from a novel perspective that treats high clouds as part of an optical continuum rather than entities with fixed opacity. The positive feedback differs significantly from previous estimates and leads to a  $0.3 \text{ }^\circ\text{C}$  increase in climate sensitivity relative to a previous community assessment.

001  
002  
003  
004 Anvil cloud thinning implies greater climate  
005  
006 sensitivity  
007

008 Adam B. Sokol<sup>1\*</sup>, Casey J. Wall<sup>2</sup> and Dennis L. Hartmann<sup>1</sup>

009 <sup>1</sup>Department of Atmospheric Sciences, University of Washington,  
010 Seattle, WA, USA.

011 <sup>2</sup>Department of Geosciences, University of Oslo, Oslo, Norway.

012 \*Corresponding author(s). E-mail(s): [abs66@uw.edu](mailto:abs66@uw.edu);  
013

014 **Abstract**

015 High clouds produced by tropical convection are expected to shrink in  
016 area as climate warms, and the radiative feedback associated with this  
017 change has long been the subject of controversy. In a recent assess-  
018 ment of climate sensitivity, the World Climate Research Programme  
019 (WCRP) estimated that this feedback is substantially negative, albeit  
020 with substantial uncertainty. Here we show that such a negative feed-  
021 back is not supported by an ensemble of high-resolution atmospheric  
022 models. Rather, the models suggest that changes in cloud area and  
023 opacity act as a modest positive feedback. The positive opacity com-  
024 ponent arises from the disproportionate reduction in the area of thick,  
025 climate-cooling clouds relative to thin, climate-warming clouds. This  
suggests that thick cloud area is tightly coupled to the rate of con-  
vective overturning—which is expected to slow with warming—whereas  
thin cloud area is influenced by other, less certain processes. The cloud  
response is examined from a novel perspective that treats high clouds  
as part of an optical continuum rather than entities with fixed opac-  
ity. The positive feedback differs significantly from previous estimates  
and leads to a +0.3 °C shift in the median estimate of equilib-  
rium climate sensitivity relative to a previous community assessment.

026 **Keywords:** cloud feedback, climate sensitivity, tropical convection  
027  
028

2 *Anvil cloud thinning implies greater climate sensitivity*

029 Anvil clouds produced by deep convection are widespread in the Tropics and  
030 are a leading source of uncertainty in the recent assessment of climate sensi-  
031 tivity by the WCRP [1]. Thermodynamic arguments predict that anvil cloud  
032 area decreases as the surface warms [2, 3], but this could produce a positive,  
033 negative, or neutral radiative feedback, since, unlike other cloud types, anvils  
034 can have both a positive or negative cloud radiative effect (CRE) at different  
035 stages of their life cycle [4, 5]. Deep convective towers and fresh, thick anvils  
036 have a high albedo and a strong, negative CRE, while thinner, aged anvils exert  
037 a modest, positive CRE [6]. Previous estimates of the anvil area feedback are  
038 altogether inconclusive; nevertheless, the maximum likelihood value assessed  
039 by the WCRP was substantially negative ( $-0.2 \text{ W/m}^2/\text{K}$ , with a Gaussian  
040 standard deviation of  $0.2 \text{ W/m}^2/\text{K}$ ). Here, we will show that such a negative  
041 feedback is not supported by an ensemble of state-of-the-art, cloud-resolving  
042 models (CRMs). To the contrary, the models predict that reductions in high  
043 cloud area come mostly from thick, reflective anvil clouds that cool the cli-  
044 mate. The clouds left behind are optically thinner on average and have a more  
045 positive climatological CRE.

046 Previous work examining the relationship between surface temperature  
047 ( $T_s$ ) and convective cloud area generally supports a reduction in cloud area  
048 with warming, albeit with regional and methodological sensitivities [7–17].  
049 Estimates of the associated radiative feedback, however, range from signifi-  
050 cantly negative [11, 14, 18] to nearly neutral [7] or slightly positive [17, 19–22].  
051 This continued uncertainty may arise, in part, from the use of various cloud  
052 classifications (e.g., cirrus, high cloud, anvil, stratiform, etc.) based on arbi-  
053 trary thresholds that vary from study to study. In reality, tropical convection  
054 generates a continuum of ice clouds, with thick cumulonimbi on one end and  
055 thin cirrus on the other. This continuum perspective is valuable because it  
056

057 reflects real physical processes—the production, gradual thinning, and even-  
058 tual dissipation of ice clouds—and provides an intuitive way of understanding  
059 the role of convectively generated clouds in tropical climate.

060 Here, we examine the ice cloud continuum using ice water path (IWP)  
061 as a coordinate. IWP—the total mass of condensed ice in the atmospheric  
062 column—can be estimated from satellite observations, is easily calculated from  
063 model output, and is closely linked to CRE and cloud optical depth ( $\tau$ ; Fig.  
064 S1). Changes in the frequency distribution of IWP are therefore informative  
065 for understanding the impact of ice clouds on the top-of-atmosphere radiative  
066 balance.

067 We apply the continuum perspective to an ensemble of cloud-resolving  
068 models (CRMs) in which deep convection and anvil evolution are explicitly  
069 simulated. As part of the Radiative-Convective Equilibrium Model Intercom-  
070 parison Project (RCEMIP) [23], these models were run on a limited-area,  
071 oceanic domain large enough to permit large-scale convective organization  
072 (Methods). Simulations were conducted for three fixed, uniform  $T_s$  values (295,  
073 300, and 305 K). We will show that the ice cloud response to warming is char-  
074 acterized by two regimes: a robust reduction in thick ice cloud area that is  
075 consistent with existing thermodynamic arguments, and a small but uncertain  
076 change in thin ice cloud area. Such changes produce an overall thinning of the  
077 cloud population and a positive opacity feedback, implying a +0.3 °C shift in  
078 the WCRP estimate of equilibrium climate sensitivity.

079

## 080 **Results**

081

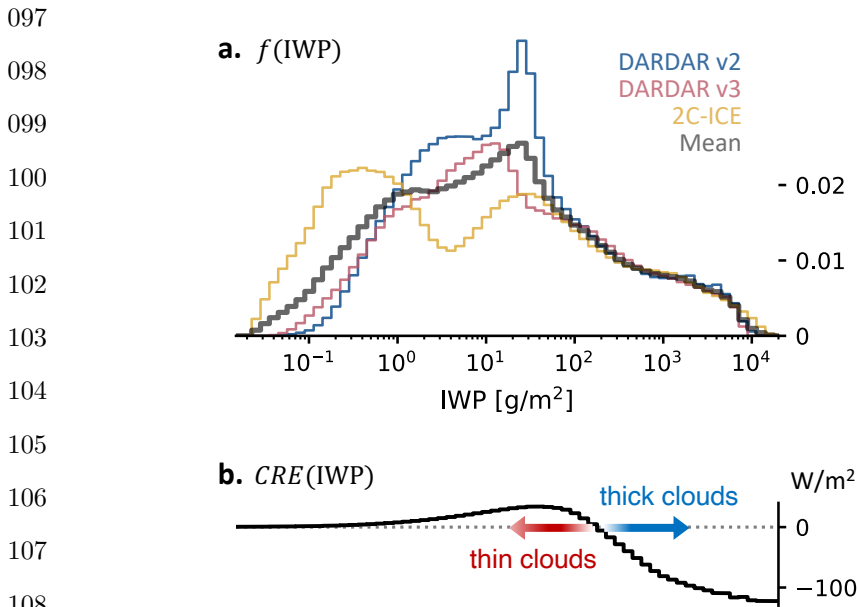
### 082 **Convective clouds as a continuum of ice**

083

083 The continuum of tropical ice clouds can be represented by a discrete frequency  
084 distribution of IWP [24, 25]. We denote this distribution as  $f(\text{IWP})$ , which

4 *Anvil cloud thinning implies greater climate sensitivity*

085 can be interpreted as the IWP-resolved cloud fraction. Similarly, we denote  
 086 the mean CRE of convectively generated ice clouds as  $CRE(IWP)$  (Methods).  
 087 Satellite-derived estimates of  $f$  from the tropical West Pacific, along with  
 088 model-estimated  $CRE$ , provide an intuitive understanding of convective cloud  
 089 evolution (Fig. 1). At high IWP ( $> 10^3 \text{ g/m}^{-2}$ ), deep convective cores have a  
 090 large, negative CRE but cover a small area. As IWP decreases,  $f$  and  $CRE$   
 091 both increase rapidly, which reflects the thinning and spreading of detrained  
 092 anvils. Maximum  $f$  occurs around  $15\text{-}35 \text{ g/m}^2$  ( $\tau \sim 1\text{-}2$ ; Supplementary Fig. 1),  
 093 which approximately coincides with the maximum  $CRE$ ; the most abundant  
 094 anvil clouds are therefore those with the strongest warming effect. These clouds  
 095 counteract the cooling effect of thicker clouds, leading to a climatological CRE  
 096 near zero in tropical convective regions [26, 27].



109 **Fig. 1 The tropical ice cloud continuum.** (a)  $f(IWP)$  derived from satellite observations  
 110 of the tropical West Pacific ( $150\text{-}180^\circ\text{E}$ ,  $15^\circ\text{S}\text{-}15^\circ\text{N}$ ) for 2009. Three satellite retrievals  
 111 and their mean are shown (Methods). (b) Multimodel mean  $CRE(IWP)$  for the CRM sim-  
 112 ulations with  $T_s=300 \text{ K}$ . Low cloud effects are treated as described in Methods.

113 The CRM ensemble produces a wide variety of IWP distributions with  
 114 varying degrees of similarity to the satellite-derived  $f$  (Fig. 2). Several aspects  
 115 of the observed distribution are well reproduced by the models: the maximum  
 116 IWP of  $2\text{--}4 \times 10^4 \text{ g/m}^2$ , the inflection point around  $10^3 \text{ g/m}^2$ , and the rapid  
 117 increase in  $f$  as IWP decreases from there. Most of the models are therefore  
 118 capturing the basic thinning and spreading of anvil clouds after detrainment.  
 119 Their performance is more mixed when it comes to the observed maximum at  
 120  $15\text{--}35 \text{ g/m}^2$ , with about half producing a relative maximum or plateau within  
 121 the observed range. That half of the models place the peak within the narrow  
 122 IWP range constrained by observations suggests that the physical processes

123

124

125

126

127

128

129

130

131

132

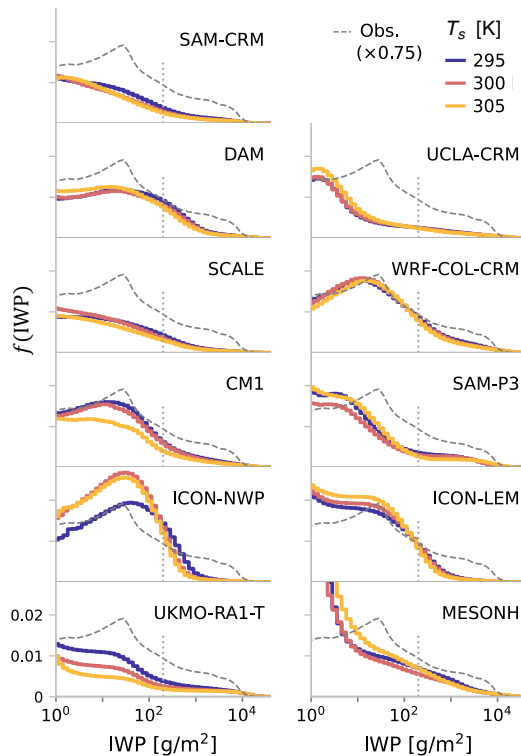
133

134

135

136

137



138 **Fig. 2 Model representations of the ice cloud continuum.** Panels show the IWP  
 139 distributions  $f(\text{IWP})$  for each model and each  $T_s$ . Dashed grey lines show the mean of the  
 140 three satellite-derived estimates of  $f$ , scaled arbitrarily by a factor of 0.75 to aid comparison  
 of distribution shapes. Vertical, dotted grey lines mark the cutoff between thick and thin  
 clouds.

141 responsible for the maximum can be captured even in idealized representations  
 142 of the tropical atmosphere.

143 In the deep Tropics, the ice cloud continuum is dominated by clouds with  
 144 tops near the level of deep convective detrainment [28]. Mid-level ice clouds  
 145 are very rare in the observations and model simulations considered here (Sup-  
 146plementary Figs. 2-3), so we are confident that  $f$  reflects a continuum of high  
 147 clouds consisting of deep convective towers, their attached anvils, and thin cir-  
 148rus of convective or in-situ origin (Supplementary Fig. 4). Based on Fig. 1,  
 149 the continuum can be divided into two categories with physical relevance for  
 150 cloud-climate interactions: clouds with  $CRE < 0$  and those with  $CRE > 0$ .  
 151 We refer to these as thick and thin clouds, respectively, and separate them by  
 152 an IWP threshold corresponding to the change in sign of the multimodel mean  
 153  $CRE$ . The area fractions covered by thick and thin clouds are then

$$f_{\text{thick}} = \sum_{200 \text{ g/m}^2}^{\infty} f$$

$$f_{\text{thin}} = \sum_{1 \text{ g/m}^2}^{200} f$$

159 and the total ice cloud fraction is  $f_{\text{ice}} = f_{\text{thick}} + f_{\text{thin}}$ . Clouds with  $\text{IWP} < 1$   
 160  $\text{g/m}^2$  have a small CRE and are excluded from our analysis, which does not  
 161 affect our results (Supplementary Discussion 1).

162 The domain-averaged CRE of ice clouds, denoted here as  $C_{\text{ice}}$ , can be sim-  
 163 ilarly decomposed into thick- and thin-cloud contributions,  $C_{\text{thick}}$  and  $C_{\text{thin}}$ ,  
 164 respectively. We first define the area-weighted CRE as

$$C(\text{IWP}) = f \cdot CRE \tag{1}$$

168



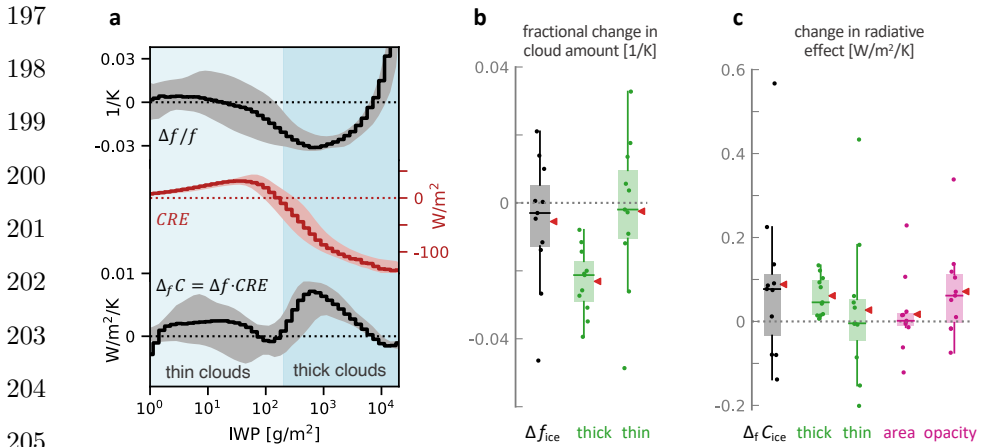
169 which represents the CRE of a particular IWP bin averaged over the entire  
170 domain. Then, as with  $f$ ,  $C_{ice}$ ,  $C_{thick}$ , and  $C_{thin}$  are found by summing  $C$  over  
171 the relevant IWP intervals (Methods; Supplementary Fig. 5).

172

## 173 Ice cloud thinning in response to warming

174 The response of  $f$  to surface warming varies substantially across the ensemble  
175 (Fig. 2a, Supplementary Figs. 6-7). To identify robust aspects of the response,  
176 we compute the multimodel mean fractional change in  $f$  between 295–305 K  
177 (Fig. 3a). This shows that  $f$  increases with warming at the largest IWPs,  
178 reflecting an increase in the ice content of the strongest convective updrafts.  
179 Otherwise, we find that thick clouds consistently contract across the entire  
180 ensemble, with a mean change in  $f_{thick}$  of  $-2\%/K$ . This change, reflective  
181 of a decrease in the area occupied by deep convective cores and fresh anvils,  
182 is in line with the anticipated weakening of the mean convective mass flux  
183 [29–31]. In theory, this weakening could manifest as a decrease in the con-  
184 vective area fraction, a decrease in the vertical velocity within convection, or  
185 some combination thereof. Since convective storms are expected to be *more*  
186 vigorous with warming [32, 33], it seems likely that convective area fraction  
187 decreases. This could arise from a reduction in the number of convective events  
188 or a decrease in their typical width, but the present analysis does not discern  
189 between these two mechanisms. Regardless, the reduction in  $f_{thick}$  seen here  
190 suggests that changes in convective area fraction affect not only deep convec-  
191 tive cores, but also fresh, thick anvil clouds, which are typically attached to  
192 convective cores and undergo relatively rapid thinning after their formation  
193 [34, 35]. The impressive agreement between the CRMs (Fig. 3b, Supplementary  
194 Fig. 6c) suggests that this response is rooted in fundamental physics shared  
195 by all of the models.

196

8 *Anvil cloud thinning implies greater climate sensitivity*

**Fig. 3** The ice cloud response to warming and its radiative effects. (a) fractional change in  $f$ (IWP),  $CRE$ (IWP) for  $T_s = 295$  K, and  $\Delta_f C$ , the change in domain-averaged CRE due to changes in  $f$  alone. Lines show multimodel means and shading shows 25-75th percentiles. (b) Fractional change in  $f_{ice}$  and its decomposition into thick- and thin-cloud components. (c) the combined area and opacity feedback  $\Delta_f C_{ice}$ , its thick- and thin-cloud components, and its area and opacity components. All changes are evaluated between 295 and 305 K and normalized by  $\Delta T_s$ . For box plots, boxes show Q1-Q3 and outliers differ from Q1 or Q3 by at least  $1.5 \times IQR$ . Dashes show medians, red triangles show means, and dots show individual models.

In contrast to the reduction in  $f_{thick}$ , there is no model consensus on changes in thin cloud area. The ensemble is evenly split on the sign of  $\Delta f_{thin}$ , resulting in a small ensemble mean response despite wide intermodel spread (Fig. 3b). The mismatch between changes in  $f_{thick}$  and  $f_{thin}$  suggests that the thin cloud response is not as tightly constrained by changes in the convective mass flux. This is in line with our current understanding that the spreading, thinning, and maintenance of aged anvils are driven by various microphysical and radiative processes that are not directly related to the total convective mass flux [4, 5, 36–38]. Intermodel differences in the representation of these processes (particularly microphysics) almost certainly impact the simulated thin cloud response. With these insights into the anvil life cycle, it is perhaps unsurprising that  $\Delta f_{thin}$  is poorly constrained compared to  $\Delta f_{thick}$ . Since thin clouds are much more abundant than thick ones (Supplementary Table 1), changes in  $f_{ice}$  largely reflect those in  $f_{thin}$  (Supplementary Table 2).

225 Intermodel spread in  $\Delta f_{\text{ice}}$  is best explained by  $\Delta f$  at  $\sim 20 \text{ g/m}^2$  ( $r^2=0.92$ ;  
 226 Supplementary Fig. 8), which closely corresponds to the most abundant IWP  
 227 in observations and some models.

228 With a robust reduction in  $f_{\text{thick}}$  and a small mean change in  $f_{\text{thin}}$ , the  
 229 ensemble suggests that the ice cloud population becomes thinner in response  
 230 to surface warming. The ratio of thin to thick clouds increases in all but one  
 231 of the models (Supplementary Fig. 7), demonstrating that this thinning can  
 232 occur regardless of whether  $f_{\text{ice}}$  increases, decreases, or stays the same. The  
 233 thinning is qualitatively consistent with recent observational and model-based  
 234 analyses [8, 16, 21, 39, 40].

235

## 236 A positive opacity feedback

237 We now seek to understand how changes in the ice cloud continuum affect  
 238  $C_{\text{ice}}$ , the domain-averaged CRE of ice clouds. The change in  $C$  due solely to  
 239 changes in  $f$  is expressed as

240

$$241 \quad \Delta_f C(\text{IWP}) = CRE \cdot \Delta f \quad (2)$$

242

243 where  $\Delta_f$  denotes the change due to  $f$  alone, normalized by  $\Delta T_s$ , and  $CRE$  is  
 244 evaluated at the initial  $T_s$ . As before,  $\Delta_f C_{\text{thick}}$ ,  $\Delta_f C_{\text{thin}}$ , and  $\Delta_f C_{\text{ice}}$  are found  
 245 by summing  $\Delta_f C$  over the respective IWP intervals.  $\Delta_f C_{\text{ice}}$  can be interpreted  
 246 as a combined area and opacity feedback, although it neglects the part of the  
 247 opacity feedback related to changes in cloud microphysics (Methods).

248 We assess  $\Delta_f C$  and  $\Delta_f C_{\text{ice}}$  separately for each model between 295–305  
 249 K. All but three produce positive  $\Delta_f C_{\text{ice}}$  (Fig. 3c), demonstrating that cloud  
 250 thinning can lead to an increase in climatological CRE regardless of whether  
 251  $f_{\text{ice}}$  increases or decreases. The ensemble mean  $\Delta_f C_{\text{ice}}$  is  $+0.09 \text{ W/m}^2/\text{K}$ ;

252

253 nearly all of this increase comes from thick cloud changes, while the mean  
254 thin-cloud contribution is again very small but with considerably more spread  
255 (Fig. 3, Supplementary Fig. 6d). Intermodel spread in  $\Delta_f C_{\text{ice}}$  is well explained  
256 by its thin-cloud component ( $r^2=0.95$ ) and best predicted by  $\Delta_f C$  at 40-70  
257  $\text{g}/\text{m}^2$  ( $r^2=0.97$ ; Supplementary Fig. 8).

258  $\Delta_f C_{\text{ice}}$  can be decomposed into two parts analogous to conventional cloud  
259 area and opacity feedbacks (Methods). The area component assumes a uniform  
260 fractional change in  $f$  and no change in  $\overline{CRE}$ , the conditionally averaged CRE  
261 of ice clouds. In most of the models, the area component is very small (Fig.  
262 3c), either because  $\Delta f_{\text{ice}}$  is small or because the ice cloud population is about  
263 radiatively neutral to begin with. This is in line with previous arguments  
264 suggesting that the radiative neutrality of convective clouds constrains the  
265 area feedback to be small [41].

266 The opacity component of  $\Delta_f C_{\text{ice}}$  accounts for changes in  $\overline{CRE}$  brought  
267 about by nonuniform changes in  $f$ , such as the thinning of the cloud population  
268 described above. Unlike the area component, the opacity component is gener-  
269 ally positive across the ensemble (Fig. 3c), reflecting a mean increase in  $\overline{CRE}$   
270 due to cloud thinning. The multimodel-mean opacity component accounts for  
271 nearly all of the magnitude of  $\Delta_f C_{\text{ice}}$ , suggesting that when it comes to anvil  
272 radiative feedbacks, shifts in opacity are more important than changes in total  
273 area. The CRMs show impressive agreement in this regard, as does at least  
274 one general circulation model with parameterized convection [21]. Again, inter-  
275 model spread in the area and opacity components is well explained by the  
276 spread in  $\Delta f_{\text{thin}}$  (Supplementary Fig. 9).

277

278

279

280

## 281 **Implications for climate sensitivity**

282 The positive anvil area and opacity feedback predicted by the CRM ensemble  
283 represents a significant departure from the WCRP estimate (Supplementary  
284 Discussion 2) and suggests that clouds act to enhance global warming more  
285 than is assumed in the WCRP assessment of equilibrium climate sensitivity  
286 (ECS). To update that assessment, we replace the previous feedback estimate  
287 with our RCEMIP-informed value and generate a new probability density func-  
288 tion (PDF) of ECS. We calculate the RCEMIP-informed value by converting  
289 the multimodel mean  $\Delta_f C_{ice}$  to a global mean feedback (Methods). This gives  
290 a feedback estimate of  $N(0.03, 0.06)$  W/m<sup>2</sup>/K, where, following the WCRP  
291 convention [1],  $N(x, y)$  is a Gaussian with mean  $x$  and standard deviation  $y$ ,  
292 which we set equal to the feedback standard deviation across the RCEMIP  
293 ensemble. While the RCEMIP-informed feedback is small in magnitude com-  
294 pared to other cloud feedbacks, it is a large change from the previous estimate  
295 and corresponds to a 51% increase in the WCRP-assessed total cloud feedback.

296 Updating the feedback results in a broad +0.3 °C shift in the ECS PDF  
297 (Fig. 4). The central estimate (median) increases from 3.1 to 3.4 °C, and the  
298 66% likely range from 2.6-3.9 to 2.8-4.2 °C (Supplementary Table 3). The  
299 ~10% widening of the likely range is counterintuitive given the reduction in  
300 anvil feedback uncertainty relative to the WCRP assessment. The reduction  
301 in uncertainty is outweighed by the increase in the central estimate of the  
302 feedback, which acts to broaden the PDF due to the nonlinear relationship  
303 between ECS and feedback strength [42]. The likelihoods of extreme ECS  
304 values are most dramatically affected by the feedback update: the probability  
305 of  $ECS > 6$  °C doubles, while that of  $ECS < 2$  °C is reduced by 74%. Sensitivity  
306 tests (Methods) show that the shift in the PDF results from the increase in  
307

308

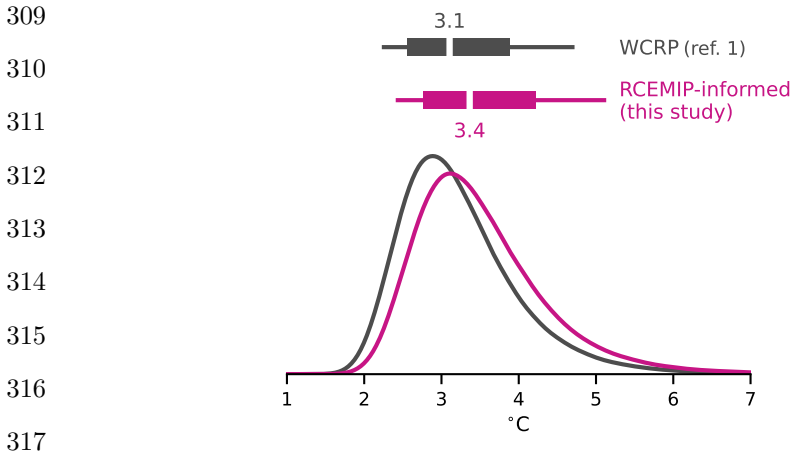


**Fig. 4 Updating the probability density function of ECS.** Grey: WCRP baseline estimate from [1], which uses an anvil area feedback of  $N(-0.20, 0.20)$   $\text{W/m}^2/\text{K}$ , where  $N(x, y)$  is a Gaussian with mean  $x$  and standard deviation  $y$ . Pink: updated calculation using the RCEMIP-informed value of  $N(0.03, 0.06)$   $\text{W/m}^2/\text{K}$ . Above, the thin horizontal lines and boxes show 90% and 66% confidence intervals, respectively, and white dashes show the central estimate (median).

the central estimate of the feedback and is quite insensitive to the feedback uncertainty (Supplementary Fig. 10, Supplementary Table 3).

Extrapolating from RCEMIP to a global mean feedback comes with the caveat that certain atmospheric changes cannot be captured in such idealized simulation setups. For example, our feedback estimate cannot account for warming-induced changes in planetary-scale circulation or dynamical modes of variability, which could affect patterns of convection and cloudiness. However, the RCEMIP CRMs produce a wide range of changes in large-scale convective organization in response to warming [43]; these changes freely affect cloud properties and are thus implicitly included in our analysis. We are therefore confident that our estimate spans a wide range of possible changes in large-scale convective dynamics. Furthermore, we have already shown that the CRMs capture the expected reduction in deep convective area in response to warming; this, along with previous work showing that the ensemble-predicted changes in

337 cloud altitude and temperature are consistent with observational and theoret-  
338 ical expectations [43, 44], adds confidence that the most fundamental aspects  
339 of the convective response are well represented by the CRMs.

340

## 341 Discussion

342 A main takeaway of this work is that changes in tropical ice cloud opacity  
343 are a critical part of the cloud response to warming. The possibility of a high  
344 cloud opacity feedback has been noted before [18, 21, 45] but has received  
345 comparatively little attention in broader discussions of cloud feedback and  
346 ECS. Previous assessments have often assumed fixed anvil opacity [11, 20],  
347 perhaps due to the lack of *a priori* expectations for how changes in area would  
348 be spread across the distribution of clouds observed in the present-day Tropics.  
349 By treating tropical ice clouds as a continuum, this work provides an initial  
350 characterization of that response. While our estimate of the combined area and  
351 opacity feedback is small, it constitutes a significant increase from the WCRP  
352 estimate [1] and implies a substantial shift in the PDF of ECS.

353 The continuum framework has revealed that thick, climate-cooling and  
354 thin, climate-warming clouds are affected differently by changes in  $T_s$ . The  
355 robust decrease in thick cloud area mirrors expected changes in convective mass  
356 flux, whereas the uncertain thin-cloud response appears to be influenced by  
357 other factors. In particular, thin clouds with IWP between 20-70 g/m<sup>2</sup> ( $\tau \sim 1-3$ )  
358 are the leading source of uncertainty in changes in ice cloud area and radiative  
359 effect. These clouds are known to be shaped by various radiative, dynamic,  
360 and microphysical processes that may respond to warming in complex ways  
361 [46]. Constraining these changes is a challenging undertaking that requires  
362 consideration of a wide range of physical scales, but such an endeavor may  
363 prove critical for understanding tropical climate change.

364

365 **Corresponding Author.** All correspondence and requests for materials  
366 should be addressed to Adam B. Sokol (abs66@uw.edu).

367 **Acknowledgments.** We thank three anonymous reviewers for their helpful  
368 feedback, Catherine Stauffer for processing and sharing RCEMIP data, Lily  
369 Hahn for helpful feedback on this manuscript, and Jakob Deutloff for helpful  
370 conversations about the treatment of cloud overlap. We acknowledge the many  
371 scientists who provided simulations for RCEMIP and the German Climate  
372 Computing Center (DKRZ) for hosting the standardized RCEMIP data. This  
373 work was supported by NASA FINESST grant 80NSSC20K1613 and NSF  
374 grant AGS-2124496.

375 **Author Contributions.** A.B.S. conceived the project, conducted the anal-  
376 ysis, generated the figures, and wrote the manuscript. C.J.W. ran the  
377 equilibrium climate sensitivity code and provided interpretation. D.L.H. inter-  
378 preted results, contributed to manuscript revision, and supervised all aspects  
379 of the project.

381 **Supplementary information.** Supplementary Discussions 1-2, Figures 1-  
382 13, and Tables 1-3.

383

## 384 **References**

385 [1] Sherwood, S. C. *et al.* An Assessment of Earth's Climate Sensitivity  
386 Using Multiple Lines of Evidence. *Reviews of Geophysics* **58** (4) (2020).  
387 <https://doi.org/10.1029/2019RG000678> .

388

389 [2] Zelinka, M. D. & Hartmann, D. L. Why is longwave cloud feedback  
390 positive? *Journal of Geophysical Research Atmospheres* **115** (16) (2010).  
391 <https://doi.org/10.1029/2010JD013817> .

392



- 393 [3] Bony, S. *et al.* Thermodynamic control of anvil cloud amount. *Proceedings*  
394 *of the National Academy of Sciences* **113** (32), 8927–8932 (2016). <https://doi.org/10.1073/pnas.1601472113> .  
395
- 396 [4] Hartmann, D. L., Gasparini, B., Berry, S. E. & Blossey, P. N. The Life  
397 Cycle and Net Radiative Effect of Tropical Anvil Clouds. *Journal of*  
398 *Advances in Modeling Earth Systems* **10** (12), 3012–3029 (2018). <https://doi.org/10.1029/2018MS001484> .  
399
- 400 [5] Gasparini, B., Blossey, P. N., Hartmann, D. L., Lin, G. & Fan, J. What  
401 Drives the Life Cycle of Tropical Anvil Clouds? *Journal of Advances in*  
402 *Modeling Earth Systems* **11** (8), 2586–2605 (2019). [https://doi.org/10.](https://doi.org/10.1029/2019MS001736)  
403 [1029/2019MS001736](https://doi.org/10.1029/2019MS001736) .  
404
- 405 [6] Hartmann, D. L. & Berry, S. E. The balanced radiative effect of tropical  
406 anvil clouds. *Journal of Geophysical Research* **122** (9), 5003–5020 (2017).  
407 <https://doi.org/10.1002/2017JD026460> .  
408
- 409 [7] Ito, M. & Masunaga, H. Process-Level Assessment of the Iris Effect Over  
410 Tropical Oceans. *Geophysical Research Letters* **49** (7), e2022GL097997  
411 (2022). <https://doi.org/10.1029/2022GL097997> .  
412
- 413 [8] Kubar, T. L. & Jiang, J. H. Net Cloud Thinning, Low-Level Cloud Dimin-  
414 ishment, and Hadley Circulation Weakening of Precipitating Clouds with  
415 Tropical West Pacific SST Using MISR and Other Satellite and Reanaly-  
416 sis Data. *Remote Sensing* **11** (10), 1250 (2019). [https://doi.org/10.3390/](https://doi.org/10.3390/rs11101250)  
417 [rs11101250](https://doi.org/10.3390/rs11101250) .
- 418 [9] Saint-Lu, M., Bony, S. & Dufresne, J.-L. Observational Evidence for a  
419 Stability Iris Effect in the Tropics. *Geophysical Research Letters* **47** (14)  
420

- 421 (2020). <https://doi.org/10.1029/2020GL089059> .
- 422 [10] Saint-Lu, M., Bony, S. & Dufresne, J.-L. Clear-sky control of anvils in  
423 response to increased CO<sub>2</sub> or surface warming or volcanic eruptions. *npj*  
424 *Climate and Atmospheric Science* **5** (1), 1–8 (2022). [https://doi.org/10.](https://doi.org/10.1038/s41612-022-00304-z)  
425 [1038/s41612-022-00304-z](https://doi.org/10.1038/s41612-022-00304-z) .
- 426
- 427 [11] Lindzen, R. S., Chou, M. D. & Hou, A. Y. Does the Earth Have an  
428 Adaptive Infrared Iris? *Bulletin of the American Meteorological Soci-*  
429 *ety* **82** (3) (2001). [https://doi.org/10.1175/1520-0477\(2001\)082<0417:](https://doi.org/10.1175/1520-0477(2001)082<0417:DTEHAA>2.3.CO;2)  
430 [DTEHAA>2.3.CO;2](https://doi.org/10.1175/1520-0477(2001)082<0417:DTEHAA>2.3.CO;2) .
- 431
- 432 [12] Su, H. *et al.* Variations of tropical upper tropospheric clouds with sea  
433 surface temperature and implications for radiative effects. *Journal of*  
434 *Geophysical Research: Atmospheres* **113** (D10) (2008). [https://doi.org/](https://doi.org/10.1029/2007JD009624)  
435 [10.1029/2007JD009624](https://doi.org/10.1029/2007JD009624) .
- 436
- 437 [13] Zelinka, M. D. & Hartmann, D. L. The observed sensitivity of high  
438 clouds to mean surface temperature anomalies in the tropics. *Jour-*  
439 *nal of Geophysical Research: Atmospheres* **116** (D23) (2011). [https:](https://doi.org/10.1029/2011JD016459)  
440 [//doi.org/10.1029/2011JD016459](https://doi.org/10.1029/2011JD016459) .
- 441
- 442 [14] Choi, Y.-S. *et al.* Revisiting the iris effect of tropical cirrus clouds with  
443 TRMM and A-Train satellite data. *Journal of Geophysical Research:*  
444 *Atmospheres* **122** (11), 5917–5931 (2017). [https://doi.org/10.1002/](https://doi.org/10.1002/2016JD025827)  
445 [2016JD025827](https://doi.org/10.1002/2016JD025827) .
- 446
- 447 [15] Igel, M. R., Drager, A. J. & van den Heever, S. C. A CloudSat cloud  
448 object partitioning technique and assessment and integration of deep

- 449 convective anvil sensitivities to sea surface temperature. *Journal of Geo-*  
450 *physical Research: Atmospheres* **119** (17), 10515–10535 (2014). <https://doi.org/10.1002/2014JD021717> .
- 452 [16] Liu, R. *et al.* High cloud variations with surface temperature from 2002  
453 to 2015: Contributions to atmospheric radiative cooling rate and precipi-  
454 tation changes. *Journal of Geophysical Research: Atmospheres* **122** (10),  
455 5457–5471 (2017). <https://doi.org/10.1002/2016JD026303> .
- 457 [17] McKim, B., Bony, S. & Dufresne, J.-L. Physical and obser-  
458 vational constraints on the anvil cloud feedback. Preprint at  
459 [https://www.authorea.com/users/538471/articles/627002-physical-](https://www.authorea.com/users/538471/articles/627002-physical-and-observational-constraints-on-the-anvil-cloud-area-feedback)  
460 [and-observational-constraints-on-the-anvil-cloud-area-feedback](https://www.authorea.com/users/538471/articles/627002-physical-and-observational-constraints-on-the-anvil-cloud-area-feedback)  
461 (2023).
- 462 [18] Mauritsen, T. & Stevens, B. Missing iris effect as a possible cause of  
463 muted hydrological change and high climate sensitivity in models. *Nature*  
464 *Geoscience* **8** (5), 346–351 (2015). <https://doi.org/10.1038/ngeo2414>.
- 466 [19] Chambers, L. H., Lin, B. & Young, D. F. Examination of New CERES  
467 Data for Evidence of Tropical Iris Feedback. *Journal of Climate* **15** (24),  
468 3719–3726 (2002). [https://doi.org/10.1175/1520-0442\(2002\)015<3719:](https://doi.org/10.1175/1520-0442(2002)015<3719:EOONCDF>2.0.CO;2)  
469 [EOONCDF>2.0.CO;2](https://doi.org/10.1175/1520-0442(2002)015<3719:EOONCDF>2.0.CO;2) .
- 470 [20] Lin, B., Wielicki, B. A., Chambers, L. H., Hu, Y. & Xu, K.-M. The  
471 Iris Hypothesis: A Negative or Positive Cloud Feedback? *Journal*  
472 *of Climate* **15** (1), 3–7 (2002). URL [https://journals.ametsoc.org/](https://journals.ametsoc.org/view/journals/clim/15/1/1520-0442_2002_015_0003_tihano_2.0.co_2.xml)  
473 [view/journals/clim/15/1/1520-0442\\_2002\\_015\\_0003\\_tihano\\_2.0.co\\_2.xml](https://journals.ametsoc.org/view/journals/clim/15/1/1520-0442_2002_015_0003_tihano_2.0.co_2.xml).  
474 [https://doi.org/10.1175/1520-0442\(2002\)015<0003:TIHANO>2.0.CO;2](https://doi.org/10.1175/1520-0442(2002)015<0003:TIHANO>2.0.CO;2),  
475 publisher: American Meteorological Society Section: Journal of Climate .  
476

- 477 [21] Li, R. L., Storelvmo, T., Fedorov, A. V. & Choi, Y.-S. A Positive Iris  
478 Feedback: Insights from Climate Simulations with Temperature-Sensitive  
479 Cloud–Rain Conversion. *Journal of Climate* **32** (16), 5305–5324 (2019).  
480 URL <http://journals.ametsoc.org/doi/10.1175/JCLI-D-18-0845.1>. <https://doi.org/10.1175/JCLI-D-18-0845.1>.  
481 <https://doi.org/10.1175/JCLI-D-18-0845.1>, publisher: American Meteorologi-  
482 cal Society .
- 483 [22] Williams, I. N. & Pierrehumbert, R. T. Observational evidence against  
484 strongly stabilizing tropical cloud feedbacks. *Geophysical Research Letters*  
485 **44** (3), 1503–1510 (2017). <https://doi.org/10.1002/2016GL072202> .  
486
- 487 [23] Wing, A. A. *et al.* Radiative–convective equilibrium model intercompar-  
488 ison project. *Geoscientific Model Development* **11** (2), 793–813 (2018).  
489 <https://doi.org/10.5194/gmd-11-793-2018> .
- 490 [24] Berry, E. & Mace, G. G. Cloud properties and radiative effects of the  
491 Asian summer monsoon derived from A-Train data. *Journal of Geo-*  
492 *physical Research* **119** (15), 9492–9508 (2014). [https://doi.org/10.1002/](https://doi.org/10.1002/2014JD021458)  
493 [2014JD021458](https://doi.org/10.1002/2014JD021458) .
- 494 [25] Chen, Y.-W. *et al.* High Cloud Responses to Global Warming Simulated  
495 by Two Different Cloud Microphysics Schemes Implemented in the Nonhy-  
496 drostatic Icosahedral Atmospheric Model (NICAM). *Journal of Climate*  
497 **29** (16), 5949–5964 (2016). <https://doi.org/10.1175/JCLI-D-15-0668.1> .
- 498 [26] Ramanathan, V. *et al.* Cloud-radiative forcing and climate: Results from  
499 the earth radiation budget experiment. *Science* **243** (4887), 57–63 (1989).  
500 <https://doi.org/10.1126/science.243.4887.57> .  
501  
502  
503  
504

- 505 [27] Hartmann, D. L., Moy, L. A. & Fu, Q. Tropical Convection and the  
506 Energy Balance at the Top of the Atmosphere. *Journal of Climate*  
507 **14** (24), 4495–4511 (2001). [https://doi.org/10.1175/1520-0442\(2001\)](https://doi.org/10.1175/1520-0442(2001)014(4495:TCATEB)2.0.CO;2)  
508 [014\(4495:TCATEB\)2.0.CO;2](https://doi.org/10.1175/1520-0442(2001)014(4495:TCATEB)2.0.CO;2), publisher: American Meteorological Society  
509 Section: Journal of Climate .
- 510 [28] Stephens, G. *et al.* CloudSat and CALIPSO within the A-Train: Ten  
511 Years of Actively Observing the Earth System. *Bulletin of the American*  
512 *Meteorological Society* **99** (3), 569–581 (2018). [https://doi.org/10.1175/](https://doi.org/10.1175/BAMS-D-16-0324.1)  
513 [BAMS-D-16-0324.1](https://doi.org/10.1175/BAMS-D-16-0324.1) .
- 514 [29] Knutson, T. R. & Manabe, S. Time-Mean Response over the Trop-  
515 ical Pacific to Increased CO<sub>2</sub> in a Coupled Ocean-Atmosphere Model.  
516 *Journal of Climate* **8** (9), 2181–2199 (1995). [https://doi.org/10.1175/](https://doi.org/10.1175/1520-0442(1995)008(2181:TMROTT)2.0.CO;2)  
517 [1520-0442\(1995\)008\(2181:TMROTT\)2.0.CO;2](https://doi.org/10.1175/1520-0442(1995)008(2181:TMROTT)2.0.CO;2) .
- 518 [30] Held, I. M. & Soden, B. J. Robust Responses of the Hydrological Cycle to  
519 Global Warming. *Journal of Climate* **19** (21), 5686–5699 (2006). [https://](https://doi.org/10.1175/JCLI3990.1)  
520 [doi.org/10.1175/JCLI3990.1](https://doi.org/10.1175/JCLI3990.1), publisher: American Meteorological Society  
521 Section: Journal of Climate .
- 522 [31] Jeevanjee, N. Three Rules for the Decrease of Tropical Convection With  
523 Global Warming. *Journal of Advances in Modeling Earth Systems* **14** (11),  
524 e2022MS003285 (2022). URL [https://onlinelibrary.wiley.com/doi/abs/](https://onlinelibrary.wiley.com/doi/abs/10.1029/2022MS003285)  
525 [10.1029/2022MS003285](https://onlinelibrary.wiley.com/doi/abs/10.1029/2022MS003285). <https://doi.org/10.1029/2022MS003285>, eprint:  
526 <https://onlinelibrary.wiley.com/doi/pdf/10.1029/2022MS003285> .
- 527 [32] Singh, M. S., Kuang, Z., Maloney, E. D., Hannah, W. M. & Wolding, B. O.  
528 Increasing potential for intense tropical and subtropical thunderstorms  
529 under global warming. *Proceedings of the National Academy of Sciences*  
530  
531  
532

533 **114** (44), 11657–11662 (2017). <https://doi.org/10.1073/pnas.1707603114>

534 .

535 [33] Romps, D. M. Clausius–Clapeyron Scaling of CAPE from Analytical  
536 Solutions to RCE. *Journal of the Atmospheric Sciences* **73** (9), 3719–3737  
537 (2016). <https://doi.org/10.1175/JAS-D-15-0327.1>, publisher: American  
538 Meteorological Society Section: Journal of the Atmospheric Sciences .

540 [34] Lilly, D. K. Cirrus outflow dynamics. *Journal of the Atmospheric Sciences*  
541 **45** (10), 1594–1605 (1988). [https://doi.org/10.1175/1520-0469\(1988\)](https://doi.org/10.1175/1520-0469(1988)045(1594:COD)2.0.CO;2)  
542 [045\(1594:COD\)2.0.CO;2](https://doi.org/10.1175/1520-0469(1988)045(1594:COD)2.0.CO;2) .

543 [35] Jensen, E. J., van den Heever, S. C. & Grant, L. D. The Life Cycles of  
544 Ice Crystals Detrained From the Tops of Deep Convection. *Journal of*  
545 *Geophysical Research: Atmospheres* **123** (17), 9624–9634 (2018). [https:](https://doi.org/10.1029/2018JD028832)  
546 [//doi.org/10.1029/2018JD028832](https://doi.org/10.1029/2018JD028832), publisher: Blackwell Publishing Ltd .

548 [36] Schmidt, C. T. & Garrett, T. J. A Simple Framework for the Dynamic  
549 Response of Cirrus Clouds to Local Diabatic Radiative Heating. *Journal*  
550 *of the Atmospheric Sciences* **70** (5), 1409–1422 (2013). [https://doi.org/](https://doi.org/10.1175/JAS-D-12-056.1)  
551 [10.1175/JAS-D-12-056.1](https://doi.org/10.1175/JAS-D-12-056.1) .

552 [37] Wall, C. J. *et al.* Observational Evidence that Radiative Heating Modifies  
553 the Life Cycle of Tropical Anvil Clouds. *Journal of Climate* **33** (20),  
554 8621–8640 (2020). <https://doi.org/10.1175/JCLI-D-20-0204.1> .

556 [38] Dobbie, S. & Jonas, P. Radiative influences on the structure and lifetime  
557 of cirrus clouds. *Quarterly Journal of the Royal Meteorological Society*  
558 **127** (578), 2663–2682 (2001). <https://doi.org/10.1002/qj.49712757808>,  
559 publisher: Wiley .

560

- 561 [39] Höjgård-Olsen, E., Chepfer, H. & Brogniez, H. Satellite Observed Sen-  
562 sitivity of Tropical Clouds and Moisture to Sea Surface Temperature on  
563 Various Time and Space Scales: 1. Focus on High Level Cloud Situations  
564 Over Ocean. *Journal of Geophysical Research: Atmospheres* **127** (6),  
565 e2021JD035438 (2022). <https://doi.org/10.1029/2021JD035438> .
- 566 [40] Stubenrauch, C. J., Caria, G., Protopapadaki, S. E. & Hemmer, F. 3D  
567 radiative heating of tropical upper tropospheric cloud systems derived  
568 from synergistic A-Train observations and machine learning. *Atmospheric*  
569 *Chemistry and Physics* **21** (2), 1015–1034 (2021). [https://doi.org/10.](https://doi.org/10.5194/acp-21-1015-2021)  
570 [5194/acp-21-1015-2021](https://doi.org/10.5194/acp-21-1015-2021) .
- 571 [41] Pierrehumbert, R. T. Thermostats, Radiator Fins, and the Local  
572 Runaway Greenhouse. *Journal of the Atmospheric Sciences* **52** (10),  
573 1784–1806 (1995). [https://doi.org/10.1175/1520-0469\(1995\)052\(1784:](https://doi.org/10.1175/1520-0469(1995)052(1784:TRFATL)2.0.CO;2)  
574 [TRFATL\)2.0.CO;2](https://doi.org/10.1175/1520-0469(1995)052(1784:TRFATL)2.0.CO;2) .
- 575 [42] Roe, G. H. & Baker, M. B. Why Is Climate Sensitivity So Unpredictable?  
576 *Science* **318** (5850), 629–632 (2007). URL [https://www.science.org/](https://www.science.org/doi/10.1126/science.1144735)  
577 [doi/10.1126/science.1144735](https://www.science.org/doi/10.1126/science.1144735). <https://doi.org/10.1126/science.1144735>,  
578 publisher: American Association for the Advancement of Science .
- 579 [43] Wing, A. A. *et al.* Clouds and Convective Self-Aggregation in a  
580 Multi-Model Ensemble of Radiative-Convective Equilibrium Simulations.  
581 *Journal of Advances in Modeling Earth Systems* (2020). [https://doi.org/](https://doi.org/10.1029/2020MS002138)  
582 [10.1029/2020MS002138](https://doi.org/10.1029/2020MS002138) .
- 583 [44] Stauffer, C. L. & Wing, A. A. Properties, Changes, and Con-  
584 trols of Deep-Convecting Clouds in Radiative-Convective Equilib-  
585 rium. *Journal of Advances in Modeling Earth Systems* **14** (6),  
586  
587  
588

589 e2021MS002917 (2022). URL [https://onlinelibrary.wiley.com/doi/abs/](https://onlinelibrary.wiley.com/doi/abs/10.1029/2021MS002917)  
 590 [10.1029/2021MS002917](https://doi.org/10.1029/2021MS002917). <https://doi.org/10.1029/2021MS002917>, eprint:  
 591 <https://onlinelibrary.wiley.com/doi/pdf/10.1029/2021MS002917> .

592 [45] Hartmann, D. L. Tropical anvil clouds and climate sensitivity. *Proceedings*  
 593 *of the National Academy of Sciences* **113** (32), 8897–8899 (2016). <https://doi.org/10.1073/pnas.1610455113> .  
 594  
 595

596 [46] Gasparini, B. *et al.* Opinion: Tropical cirrus – from micro-scale processes  
 597 to climate-scale impacts. *Atmospheric Chemistry and Physics* **23** (24),  
 598 15413–15444 (2023). <https://doi.org/10.5194/acp-23-15413-2023> .  
 599

## 600 **Methods**

### 601 **Satellite Observations of IWP**

602 The three satellite retrievals shown in Fig. 1b are combined radar-lidar  
 603 retrievals that use measurements from the CALIOP lidar [47] and the  
 604 CloudSat radar [48]. Both instruments are part of the A-train satellite  
 605 constellation. The three retrievals are DARDAR-Cloud version 2.1.1 [49],  
 606 DARDAR-Cloud version 3.1 [50], and 2C-ICE R05 [51]. The two versions  
 607 of DARDAR-Cloud differ principally in their treatment of cloudy volumes  
 608 detected by the lidar only [50].  
 609

### 610 **Cloud-resolving model ensemble**

611 We use output from the “RCE\_large” simulations of RCEMIP. The full  
 612 simulation protocol is described in [23]. Briefly, the simulations have a  
 613 domain size of  $\sim 6,000 \times 400$  km<sup>2</sup> with 3-km horizontal resolution. They  
 614 used three fixed, uniform sea surface temperatures (295, 300, and 305 K)  
 615 and were integrated for 100 days. We use the instantaneous 3D output  
 616



617 (every 6 hours) from the last 25 days of each run. Instantaneous IWP  
618 is computed by vertically integrating the total (precipitating and non-  
619 precipitating) atmospheric ice content. We included precipitating ice to  
620 be consistent with the satellite observations, which do not distinguish  
621 between ice types.

622 Our analysis includes all of the RCEMIP CRMs for which the necessary,  
623 standardized output is publicly available, with the exception of UKMO-  
624 RA1-T-nocloud and UKMO-CASIM. UKMO-RA1-T-nocloud is the same  
625 as UKMO-RA1-T apart from its deactivation of a subgrid cloud scheme.  
626 UKMO-CASIM is excluded because the unique vertical structure of con-  
627 vection in that model produces an IWP distribution that does not reflect  
628 deep convective cloud climatology, but rather expansive, stratiform ice  
629 clouds produced by convective detrainment near the freezing level. We also  
630 include the RCEMIP\_large-style simulations described in [52], which use  
631 the SAM model [53] with P3 microphysics [54] (referred to as SAM-P3).

### 632 **Calculation of $CRE(IWP)$ and treatment of low clouds**

634 For each column of model output, CRE is computed as the difference  
635 between hourly mean all-sky and clear-sky radiative fluxes. We seek to  
636 calculate  $CRE(IWP)$  such that it reflects the radiative effects of clouds  
637 produced by deep convection while excluding the effects of unrelated liq-  
638 uid clouds below. To this end, we first compute the mean CRE of all  
639 columns falling within each IWP bin (the “all-cloud” CRE) as well as  
640 that of the columns with liquid water path below 1 g/m<sup>2</sup> (the “ice-only”  
641 CRE). Liquid clouds found in low-IWP columns are typically low clouds  
642 at the top of the boundary layer, which are unrelated to the overly-  
643 ing ice clouds but nevertheless have an impact on the top-of-atmosphere  
644 CRE [55]. Therefore, to exclude their radiative effects from  $CRE(IWP)$ ,

645 we set  $CRE(IWP)$  equal to the ice-only for  $IWP < 10^2 \text{ g/m}^2$ . On the  
 646 other hand, liquid found in high-IWP columns is typically part of same  
 647 deep convective cloud as the ice above; we seek to include these liquid  
 648 effects and therefore set  $CRE(IWP)$  equal to the all-sky CRE for  $IWP$   
 649  $> 10^3 \text{ g/m}^2$ . Between  $10^2$  and  $10^3 \text{ g/m}^2$ , we use a transition that is lin-  
 650 ear with respect to  $\log_{10}IWP$  (Supplementary Fig. 11). These thresholds  
 651 were selected based on the multimodel mean liquid cloud fraction within  
 652 each IWP bin (Supplementary Fig. 12), which increases rapidly between  
 653 inflection points at  $10^2$  and  $10^3 \text{ g/m}^2$ , signaling a shift from low clouds  
 654 unrelated to the high clouds above to deep convective clouds occupying a  
 655 large portion of the atmospheric column. Our results are not sensitive to  
 656 the details of this transition, and the multimodel mean  $CRE(IWP)$  for  
 657  $T_s=295 \text{ K}$  changes sign at  $\sim 200 \text{ g/m}^2$  ( $\tau \sim 4\text{-}5$ ; Supplementary Fig. 1) ,  
 658 which is consistent with previous analyses [24, 56, 57].

## 659 **Definitions in the IWP framework**

660  
 661 We have defined  $f(IWP)$  and  $CRE(IWP)$  as the IWP-resolved cloud frac-  
 662 tion and CRE, respectively. We have also defined the area-weighted CRE  
 663 as  $C(IWP) = f(IWP) \cdot CRE(IWP)$ . For any parameter  $X(IWP)$ , we  
 664 compute the thick and thin cloud contributions to the domain mean as

$$665 \quad X_{\text{thick}} = \sum_{200 \text{ g/m}^2}^{\infty} X$$

$$666 \quad X_{\text{thin}} = \sum_{1 \text{ g/m}^2}^{200} X$$

667  
 668 and the total ice cloud contribution as  $X_{\text{ice}} = X_{\text{thick}} + X_{\text{thin}}$ . This notation  
 669  
 670 is applied to  $f(IWP)$  and  $C(IWP)$  throughout the paper, with  $f_{\text{ice}}$  and  
 671  
 672

673  $C_{\text{ice}}$  thus representing the domain-averaged ice cloud fraction and the  
 674 domain-averaged ice cloud radiative effect, respectively. The conditionally  
 675 averaged ice cloud CRE is defined as  $\overline{CRE} = C_{\text{ice}}/f_{\text{ice}}$ .

## 676 Analytical expressions for cloud feedback in the IWP

### 677 Framework

678  
 679 The Cess-type cloud feedback is defined as the change in domain-averaged  
 680 CRE normalized by  $\Delta T_s$  [58]. It differs slightly from the formal cloud  
 681 feedback parameter computed by partial radiative perturbation [59]. In  
 682 traditional feedback analysis, the total cloud feedback is often decomposed  
 683 into cloud altitude, area, and opacity components. Resolved across the  
 684 IWP continuum, the total Cess-type, ice cloud feedback is expressed as

$$685 \quad \Delta C(\text{IWP}) = CRE \cdot \Delta f + f \cdot \Delta CRE + \Delta f \cdot \Delta CRE \quad (3)$$

687  
 688 where all variables are functions of IWP and all  $\Delta$  terms are assumed to be  
 689 normalized by  $\Delta T_s$ . The final term on the right-hand side is a small non-  
 690 linear term that we neglect here. The second term on the right-hand side  
 691 accounts for changes in  $CRE(\text{IWP})$ , which may occur due to changes in  
 692 clear-sky fluxes or cloud temperature, altitude, and microphysical struc-  
 693 ture. This term encompasses so-called cloud masking effects [59], the entire  
 694 ice cloud altitude feedback, as well as the microphysical part of the opac-  
 695 ity feedback, which manifests as a change in the optical depth associated  
 696 with a particular IWP. While this term is significant (Supplementary Fig.  
 697 13), it is not our focus here.

698 The first term on the right-hand side of Eq. 2, which we define as  $\Delta_f C$ ,  
 699 is the part of  $\Delta C$  attributable to changes in the frequency of a particular

700

701 IWP.  $\Delta_f C_{\text{ice}}$ , equal to the sum of  $\Delta_f C$  across all IWP  $> 1 \text{ g/m}^2$ , is thus  
 702 the change in the domain-averaged CRE of ice clouds due to changes  
 703 in  $f$  alone.  $\Delta_f C_{\text{ice}}$  encompasses the entire ice cloud area feedback and  
 704 the remaining part of the ice cloud opacity feedback, since nonuniform  
 705 changes in  $f$  can drive changes in mean ice cloud opacity. To formally  
 706 separate the area and opacity components, we first define the fractional  
 707 change in  $f(\text{IWP})$  as

$$708 \quad g(\text{IWP}) = \frac{\Delta f}{f} \quad (4)$$

709 which can be decomposed as

$$711 \quad g(\text{IWP}) = G + g'(\text{IWP}) \quad (5)$$

713 where  $G = \Delta f_{\text{ice}}/f_{\text{ice}}$  is the fractional change in total ice cloud fraction  
 714 and  $g'$  is the deviation from  $G$  at a particular IWP. Combining equations  
 715 (4) and (5) yields

$$717 \quad \Delta f = f \cdot (G + g') \quad (6)$$

718 which when substituted into equation (2) yields

$$720 \quad \Delta_f C = C(G + g') \quad (7)$$

722 where we have employed equation (1).  $\Delta_f C_{\text{ice}}$  is then found by summing  
 723 over all IWP  $> 1 \text{ g/m}^2$ :

$$725 \quad \Delta_f C_{\text{ice}} = G \sum_{1 \text{ g/m}^2}^{\infty} C + \sum_{1 \text{ g/m}^2}^{\infty} g' C \quad (8)$$

727

728

729 which, using the definitions of  $C_{\text{ice}}$  and  $G$ , simplifies to

$$730 \quad \Delta_f C_{\text{ice}} = \Delta f_{\text{ice}} \cdot \overline{CRE} + \sum_{1 \text{ g/m}^2}^{\infty} g' C \quad (9)$$

733 The first term on the right-hand side is the area component of  $\Delta_f C_{\text{ice}}$ ,  
 734 which is attributable to changes in total ice cloud fraction assuming fixed  
 735  $\overline{CRE}$  (i.e., a uniform fractional change in  $f$  across all IWP). The second  
 736 term is the opacity component, which accounts for deviations from a uni-  
 737 form fractional change, which causes bulk thinning or thickening of the  
 738 ice cloud population and may affect  $\overline{CRE}$ . The opacity component does  
 739 not account for the microphysically driven opacity changes included in  
 740 the second term of Eq. 3.

741 Recently, [17] developed a simplified expression for the anvil cloud area  
 742 feedback (their Equation 9, which they refer to as the Iris feedback).  
 743 Unlike the Cess-type feedbacks discussed above, their expression aligns  
 744 with traditional feedback formalism. Discretizing their expression shows  
 745 that it is the same as the cloud area component of equation (9), with the  
 746 addition of a cloud overlap term. Therefore,  $\Delta_f C_{\text{ice}}$  can be interpreted  
 747 as the sum of the ice cloud area feedback and the part of the opacity  
 748 feedback related to changes in  $f$ . With regard to our treatment of cloud  
 749 overlap here, the formulation of  $CRE(\text{IWP})$  described above must be  
 750 kept in mind. Whether or not the radiative effects of cloud liquid are  
 751 included in  $\Delta_f C$  depends on IWP. At high IWPs corresponding to deep  
 752 convective cores and very thick anvil clouds, we have assumed that any  
 753 liquid present in the column belongs to the same cloud system as the ice,  
 754 and the all-sky CRE is thus used to evaluate  $\Delta_f C$ . On the other hand,  
 755 at low IWPs,  $\Delta_f C$  is evaluated using the ice-only CRE. This means, for  
 756

757 example, that the ice-free area exposed by a reduction in  $f$  is partially  
758 occupied by low clouds exerting a negative radiative effect. The low-cloud  
759 CRE in the newly exposed regions is assumed to be equal to the difference  
760 between the all-sky and ice-only CREs. This is likely an underestimate,  
761 since the CREs of overlapping low and high clouds are not simply additive  
762 in reality. However, the impact of this bias on  $\Delta_f C_{\text{ice}}$  is small due to  
763 compensating effects of models with increasing and decreasing thin cloud  
764 area. To account for this potential uncertainty, our analysis of equilibrium  
765 climate sensitivity (ECS) includes sensitivity tests, described below.

766

767

768

### **Converting $\Delta_f C_{\text{ice}}$ to a global mean feedback and estimating ECS**

769

770

771

772

773

774

775

776

777

778

779

The ensemble mean  $\Delta_f C_{\text{ice}}$  represents the anvil cloud area and opacity  
feedback, which we take to be valid over Earth's tropical oceans. To con-  
vert this to a global mean feedback, we multiply by the fractional area of  
the tropical oceans (37%) and assume that the Tropics warm by 0.9 °C  
for every degree of global mean warming [60]. This results in the reported  
feedback value of  $N(0.03, 0.06)$  W/m<sup>2</sup>/K, where the Gaussian standard  
deviation is set equal to the standard deviation of the feedback across  
the RCEMIP ensemble. We then generated updated probability density  
function of ECS using the Bayesian inference code from [1] with all three  
lines of evidence used in their original analysis (historical, process-based,  
and paleoclimatological).

780

781

782

783

784

We conduct sensitivity tests to account for additional sources of uncer-  
tainty that may not be captured by the standard deviation of the RCEMIP  
ensemble. For example, changes in cloud microphysical structure could  
contribute to the opacity feedback but are not included in our estimate

785 due to model output limitations. Overlap between high and low clouds,  
786 some of which is accounted for in our estimate, is another possible source  
787 of model bias and feedback uncertainty. To assess the impact of greater  
788 feedback uncertainty, we run the ECS calculations for additional feed-  
789 back values of  $N(0.03, 0.16)$  and  $N(0.03, 0.20)$  W/m<sup>2</sup>/K. The value of  
790 0.16 W/m<sup>2</sup>/K is the maximum deviation of any individual model from  
791 the multimodel mean and thus encompasses the full ensemble spread.  
792 The value of 0.20 W/m<sup>2</sup>/K is the WCRP-assessed uncertainty from [1],  
793 intended to serve as an upper bound. As shown in Supplementary Fig. 10  
794 and Supplementary Table 3, the resulting PDFs are very similar to that  
795 for  $N(0.03, 0.06)$ .

796 **Data availability.** The DARDAR-Cloud satellite products are avail-  
797 able at <https://www.icare.univ-lille.fr/dardar/data-access/> and the 2C-  
798 ICE products at [https://www.cloudsat.cira.colostate.edu/data-products/](https://www.cloudsat.cira.colostate.edu/data-products/2c-ice)  
799 [2c-ice](https://www.cloudsat.cira.colostate.edu/data-products/2c-ice). RCEMIP model output is publicly available at [http://hdl.handle.](http://hdl.handle.net/21.14101/d4beee8e-6996-453e-bbd1-ff53b6874c0e)  
800 [net/21.14101/d4beee8e-6996-453e-bbd1-ff53b6874c0e](http://hdl.handle.net/21.14101/d4beee8e-6996-453e-bbd1-ff53b6874c0e), and full output  
801 from the SAM-P3 model runs is available from the correspond-  
802 ing author on request. The derived data needed to reproduce the  
803 figures in this paper is available at [https://github.com/adamsokol/](https://github.com/adamsokol/Ice-cloud-feedbacks-in-RCEMIP)  
804 [Ice-cloud-feedbacks-in-RCEMIP](https://github.com/adamsokol/Ice-cloud-feedbacks-in-RCEMIP).

805 **Code availability.** The code used for the climate sensitivity calcu-  
806 lations is available from ref. 1 at [https://zenodo.org/record/3945276#](https://zenodo.org/record/3945276#.ZFvtAOzMJ8Z)  
807 [.ZFvtAOzMJ8Z](https://zenodo.org/record/3945276#.ZFvtAOzMJ8Z). Upon publication, the code needed to generate the  
808 figures in this paper will be added to the repository at [https://github.](https://github.com/adamsokol/Ice-cloud-feedbacks-in-RCEMIP)  
809 [com/adamsokol/Ice-cloud-feedbacks-in-RCEMIP](https://github.com/adamsokol/Ice-cloud-feedbacks-in-RCEMIP).

811

812

## Methods References

- 813  
814  
815 [47] Winker, D. M. *et al.* Overview of the CALIPSO Mission and  
816 CALIOP Data Processing Algorithms. *Journal of Atmospheric and*  
817 *Oceanic Technology* **26** (11), 2310–2323 (2009). [https://doi.org/10.1175/](https://doi.org/10.1175/2009JTECHA1281.1)  
818 [2009JTECHA1281.1](https://doi.org/10.1175/2009JTECHA1281.1) .
- 819 [48] Stephens, G. L. *et al.* The cloudsat mission and the A-Train: A new  
820 dimension of space-based observations of clouds and precipitation. *Bul-*  
821 *letin of the American Meteorological Society* **83** (12), 1771–1790+1742  
822 (2002). <https://doi.org/10.1175/BAMS-83-12-1771> .
- 823 [49] Delanoë, J. & Hogan, R. J. Combined CloudSat-CALIPSO-MODIS  
824 retrievals of the properties of ice clouds. *Journal of Geophysical Research:*  
825 *Atmospheres* **115** (D4) (2010). <https://doi.org/10.1029/2009JD012346> .
- 826  
827 [50] Cazenave, Q. *et al.* Evolution of DARDAR-CLOUD ice cloud retrievals:  
828 New parameters and impacts on the retrieved microphysical properties.  
829 *Atmospheric Measurement Techniques* **12** (5), 2819–2835 (2019). <https://doi.org/10.5194/amt-12-2819-2019> .
- 830  
831 [51] Deng, M., Mace, G. G., Wang, Z. & Okamoto, H. Tropical Compo-  
832 sition, Cloud and Climate Coupling Experiment validation for cirrus  
833 cloud profiling retrieval using CloudSat radar and CALIPSO lidar. *Jour-*  
834 *nal of Geophysical Research: Atmospheres* **115** (D10) (2010). <https://doi.org/10.1029/2009JD013104> .
- 835  
836  
837 [52] Sokol, A. B. & Hartmann, D. L. Congestus Mode Invigoration by  
838 Convective Aggregation in Simulations of Radiative-Convective Equilib-  
839 rium. *Journal of Advances in Modeling Earth Systems* **14** (7) (2022).  
840



- 841 <https://doi.org/10.1029/2022MS003045> .
- 842 [53] Khairoutdinov, M. F. & Randall, D. A. Cloud Resolving Modeling of the  
843 ARM Summer 1997 IOP: Model Formulation, Results, Uncertainties, and  
844 Sensitivities. *Journal of the Atmospheric Sciences* **60** (4), 607–625 (2003).  
845 [https://doi.org/10.1175/1520-0469\(2003\)060\(0607:CRMOTA\)2.0.CO;2](https://doi.org/10.1175/1520-0469(2003)060(0607:CRMOTA)2.0.CO;2) .  
846
- 847 [54] Morrison, H. *et al.* Parameterization of Cloud Microphysics Based on  
848 the Prediction of Bulk Ice Particle Properties. Part II: Case Study  
849 Comparisons with Observations and Other Schemes. *Journal of the*  
850 *Atmospheric Sciences* **72** (1), 312–339 (2015). [https://doi.org/10.1175/](https://doi.org/10.1175/JAS-D-14-0066.1)  
851 [JAS-D-14-0066.1](https://doi.org/10.1175/JAS-D-14-0066.1) .
- 852 [55] Kang, H., Choi, Y.-S., Hwang, J. & Kim, H.-S. On the cloud radiative  
853 effect for tropical high clouds overlying low clouds. *Geoscience Letters*  
854 **7** (1), 7 (2020). <https://doi.org/10.1186/s40562-020-00156-6> .  
855
- 856 [56] Hong, Y., Liu, G. & Li, J.-L. F. Assessing the Radiative Effects of  
857 Global Ice Clouds Based on CloudSat and CALIPSO Measurements.  
858 *Journal of Climate* **29** (21), 7651–7674 (2016). [https://doi.org/10.1175/](https://doi.org/10.1175/JCLI-D-15-0799.1)  
859 [JCLI-D-15-0799.1](https://doi.org/10.1175/JCLI-D-15-0799.1) .
- 860 [57] Kubar, T. L., Hartmann, D. L. & Wood, R. Radiative and Convective  
861 Driving of Tropical High Clouds. *Journal of Climate* **20** (22), 5510–5526  
862 (2007). <https://doi.org/10.1175/2007JCLI1628.1> .  
863
- 864 [58] Cess, R. D. & Potter, G. L. A methodology for understanding and  
865 intercomparing atmospheric climate feedback processes in general circu-  
866 lation models. *Journal of Geophysical Research: Atmospheres* **93** (D7),  
867 8305–8314 (1988). <https://doi.org/10.1029/JD093iD07p08305> .  
868

- 869 [59] Soden, B. J., Broccoli, A. J. & Hemler, R. S. On the Use of Cloud  
870 Forcing to Estimate Cloud Feedback. *Journal of Climate* **17** (19), 3661–  
871 3665 (2004). URL [https://journals.ametsoc.org/view/journals/clim/](https://journals.ametsoc.org/view/journals/clim/17/19/1520-0442_2004_017_3661_otuocf_2.0.co_2.xml)  
872 [17/19/1520-0442\\_2004\\_017\\_3661\\_otuocf\\_2.0.co\\_2.xml](https://journals.ametsoc.org/view/journals/clim/17/19/1520-0442_2004_017_3661_otuocf_2.0.co_2.xml). [https://doi.org/10.](https://doi.org/10.1175/1520-0442(2004)017(3661:OTUOCF)2.0.CO;2)  
873 [1175/1520-0442\(2004\)017\(3661:OTUOCF\)2.0.CO;2](https://doi.org/10.1175/1520-0442(2004)017(3661:OTUOCF)2.0.CO;2), publisher: American  
874 Meteorological Society Section: Journal of Climate .
- 875 [60] Lee, J.-Y. *et al.* in *Future Global Climate: Scenario-Based Projections and*  
876 *Near-Term Information* (eds V. Masson-Delmotte *et al.*) *Climate Change*  
877 *2021: The Physical Science Basis. Contribution of Working Group I to*  
878 *the Sixth Assessment Report of the Intergovernmental Panel on Climate*  
879 *Change* 553–672 (Cambridge University Press, Cambridge, United King-  
880 dom and New York, NY, USA, 2021). Doi: 10.1017/9781009157896.006.  
881  
882  
883  
884  
885  
886  
887  
888  
889  
890  
891  
892  
893  
894  
895  
896